Pharmaceutical Sciences. 2025;31(4):425-439
doi:10.34172/PS.025.40979
https://ps.tbzmed.ac.ir/

Research Article

A Combination Delivery of Silver and Paclitaxel in Albumin Nanoparticles for Breast Cancer Cells

Marzieh Azizi[1,2], Seyed Hossein Kiaie[3], Fatemeh Yazdian[4], Mohammad Sheibani[5,6], Bo Nyström[2], Hedayatollah Ghourchian[1*]

[1]Laboratory of Bioanalysis, Institute of Biochemistry and Biophysics, University of Tehran, Tehran, Iran
[2]Department of Chemistry, University of Oslo, Oslo, Norway
[3]Faculty of Pharmacy, Tabriz University of Medical Sciences, Tabriz, Iran
[4]Faculty of New Science and Technology, University of Tehran, Tehran, Iran
[5]Department of Pharmacology, School of Medicine, Iran University of Medical Sciences, Tehran, Iran
[6]Razi Drug Research Center, School of Medicine, Iran University of Medical Sciences, Tehran, Iran

ARTICLE INFO

Article History:
Received: November 17, 2024
Revised: February 26, 2025
Accepted: May 28, 2025
ePublished: October 11, 2025

Keywords:
Silver nanoparticles, Paclitaxel, Albumin, Combination, Apoptosis, Breast cancer

Abstract

Background: Breast cancer (BC) remains one of the most prevalent forms of cancer globally, presenting significant challenges in its treatment. The development of combination therapy utilizing nanoparticles (NPs) shows great promise in overcoming these complexities.

Methods: In our study, a composition of bovine serum albumin nanoparticles (BSANPs) loaded with paclitaxel (PTX) and silver nanoparticles (SNPs) was prepared and characterized to explore the therapeutic potential of combination drug therapy. The SNPs and PTX were incorporated into BSA NPs (SNPs-PTX@BSA) using a modified nanoprecipitation technique, resulting in uniformly sized, spherical NPs.

Results: Upon evaluating dose dependency and cytotoxicity, SNPs-PTX@BSA treatment significantly increased levels of early and late apoptosis, caused a strong arrest in the S/G2/M phases, and elevated the subG1 cell population.

Conclusion: The findings indicate that SNPs-PTX@BSA markedly affect cell death mechanisms and cell cycle regulation. Our results suggest that co-loaded delivery systems like SNPs-PTX@BSA hold significant promise as a therapeutic strategy to enhance clinical outcomes in the treatment of MDA-MB-231 invasive BC cells.

Introduction

Chemotherapy is the primary treatment for several types of cancers, but it is known for its limited effectiveness and significant systemic side effects.[1] Furthermore, drug resistance in tumors is a significant factor contributing to the limited antitumor efficacy of many drugs.[2] Tumor resistance mechanisms encompass obstacles such as high interstitial fluid pressure, which impedes the proper uptake of anticancer medications, genetic mutations that interfere with cell cycle regulation, and the active expulsion of drugs by ATP-binding cassette transporters like P-glycoprotein (P-gp).[3,4] Overexpression of the P-gp receptor has been associated with a negative prognosis in a range of cancers, including breast, ovarian, lung, and bone carcinoma.[5-8] Therefore, combination chemotherapy has been adopted to improve the efficacy of drugs while reducing side effects and showing effectiveness in treating drug-resistant cancers.[9] Breast cancer (BC) is one of the most commonly diagnosed cancers globally and a leading cause of cancer-related mortality among women. It arises from the uncontrolled growth of breast cells and can be classified into various subtypes based on hormone receptor status and genetic characteristics.[10] Despite the advancements in treatment options, a significant challenge remains the development of resistance to chemotherapy[11,12] particularly to drugs like paclitaxel (PTX), which is commonly used in BC treatment.[13] Resistance to PTX can be attributed to several mechanisms, including the overexpression of drug efflux transporters such as P-gp, which actively removes the drug from cancer cells, and alterations in microtubule dynamics affecting the PTX mechanism of action.[13-15]

Simultaneously administering drugs effectively addresses pharmacological and genetic barriers, including mutations and adaptations in tumor cells, and inhibiting drug transport.[16] PTX is a potent chemotherapy agent for solid tumors, stabilizing microtubules and causing cancer cells to arrest at the G2/M phase and triggering apoptosis.[17,18] Nevertheless, the P-gp substrate property of PTX continues to pose challenges regarding side effects

***Corresponding Author:** Hedayatollah Ghourchian, Email: ghourchian@ut.ac.ir

and hence induces overexpression of this efflux pump in patients.[19] The PTX action enhancing nuclear factor-κB (NF-κB) expression can increase the upregulation of multidrug resistance protein. Conversely, the upregulation of phosphoinositide-3-kinase (PI3K)/Akt in various malignant tumors supports cell proliferation and survival.[20] These processes can restrict the effectiveness of drug and chemotherapeutic applications of PTX.[21] Furthermore, nanoparticles (NPs), such as bovine serum albumin NPs (BSANPs), as biodegradable, biocompatible, and non-toxic particles with no immunogenic protein effect, have been demonstrated to enhance PTX efficacy.[22,23]

Silver nanoparticles (SNPs), an FDA-approved nanomaterial, demonstrate anticancer activity by triggering various apoptotic signaling pathways that promote programmed cell death.[24] To this end, SNPs can induce apoptosis in NIH3T3 cells by increasing reactive oxygen species (ROS) generation and activating the c-Jun NH2-terminal kinase (JNK) pathway, which leads to mitochondria-dependent apoptosis.[25] Numerous studies have demonstrated that nanocarriers can improve the delivery of chemotherapeutic agents, increase their bioavailability, and enable targeted delivery to tumor sites. For example, the integration of SNPs with chemotherapy agents has shown promising results in the efficacy of cancer treatment.[26] Studies show that SNPs improve the effectiveness of cisplatin,[27] and doxorubicin[28] in cancer models, enhancing apoptosis in cancer cells. Moreover, combination studies demonstrate that SNPs improve the anticancer activity of PTX in several tumors, leading to greater efficacy and reduced tumor sizes in animal models.[29,30] In light of the apoptotic role of SNPs and our prior research on utilizing BSA NPs-loaded SNPs to improve antitumor effectiveness, cellular uptake, and drug release.[31] We have designed a novel research study that focuses on delivering a combination of hydrophobic chemotherapy agent (PTX) and hydrophilic silver agents using BSANPs. This formulation, SNPs-PTX@BSA, is specifically aimed at targeting MDA-MB-231 invasive BC cells.

Materials and Methods

Materials

PTX was purchased from Jiangsu Yew Pharmaceutical Co., Ltd. (China). BSA (MW = 66 000), FBS, and Dulbecco's modified eagle medium (DMEM) were obtained from Gibco (United States). 3-(4,5-Dimethylthiazol-2-yl)-2,5-diphenyl tetrazolium bromide (MTT), 4′,6-Diamidino-2-phenylindole (DAPI), 7-Amino-actinomycin (7-AAD), Propidium iodide (PI), Penicillin, and Streptomycin were sourced from Sigma (United Kingdom). Silver nitrate ($AgNO_3$) was supplied by Merck Chemicals (Germany). The MDA-MB-231 BC cells were obtained from the National Cell Bank at the Pasteur Institute of Iran.

Methods

Preparation and characterization of SNPs

The silver colloid was synthesized using a chemical reduction approach.[32] Briefly, 50 mL $AgNO_3$ (1 mM) was boiled, then 5 mL of 1% trisodium citrate was added dropwise until the solution color changed to pale yellow. The sample was then removed from the heat and stirred until it cooled to room temperature (RT). Characterization was performed using a dynamic light scattering (DLS) analyzer (90Plus PALS, Brookhaven, USA) to measure hydrodynamic size, polydispersity index (PDI), and zeta potential (ZP). ZP measurements were conducted with a Brookhaven 90 Plus phase analysis light scattering (PALS) instrument (Brookhaven Instruments Corporation, USA) using Particle Sizing & PALS analyzer software, which calculates the ZP from the PALS data. Additionally, scanning electron microscopy (SEM) (Zeiss, DSM-960A) and transmission electron microscopy (TEM) (JEOL JEM 1400 equipped with a TVIPS TemCam-F216 camera) were utilized for high-magnification imaging of the SNPs.

PTX and SNPs synergism

A design of experiment (DOE) model was employed for data analysis, as well as to determine the optimal concentrations of SNPs and PTX. A full second-order polynomial model was developed using multiple regression techniques for three factors with Design Expert software (Minneapolis, USA, Version 7.0). This statistical package was utilized to describe the response surface methodology (RSM).

Preparation and characterization of SNPs-PTX@BSA NPs

According to the DOE, the ratio of PTX to SNPs was fixed within the range of 1.03 to 5.75 across all experiments (Table S1D). Additionally, the concentration of BSA (1-5%), the ratio of BSA to anticancer agents (1-9%), and pH (5.4-7.7) were considered variable factors (Table S2). SNPs-PTX@BSA NPs were synthesized using two solutions, designated A and B. Solution A was prepared by dissolving BSA and SNPs in 1000 µL of a PBS:dichloromethane (DCM) mixture (99:1 v/v). The concentrations of BSA and SNPs are detailed in Table S2B. Solution B was prepared by dissolving PTX in a mixture of 20 µL of absolute ethanol and 230 µL of DCM, with the PTX concentration also specified (Table S2B).

Solution B was added dropwise to solution A, and the mixture was gently agitated for 5 min. Once a crude emulsion formed, the material was transferred to a high-pressure homogenizer (Bandelin Sonopuls, Germany). The emulsification was conducted at 20 kHz at RT until a milky suspension was achieved. Subsequently, the mixture was moved to a rotary evaporator, and DCM was rapidly evaporated for 20-30 min at 40 °C (30 mm Hg). The ZP of the suspended particles was determined using a Zetaplus ZP analyzer (Brookhaven Instruments). At the same time, the morphology of SNPs-PTX@BSA NPs was analyzed using a TEM instrument (80 kV voltage).

Spectrophotometry

UV-Vis spectroscopy was conducted using a Carey 100

Bio instrument from Varian, Australia, with Cary WinUV software. Before measurement, the SNPs-PTX@BSA NPs were diluted to a final concentration of 40 mM in 0.1 M pH 7.4 PBS. Absorbance spectra were recorded over a wavelength range of 200-800 nm with a scan speed of 600 nm/min, using a quartz cuvette with a path length of 1 cm for all measurements. Baseline correction was performed with a blank sample containing only 0.1 M PBS (pH 7.4)

In vitro cytotoxicity assay

The MDA-MB-231 cells were cultured in a DMEM medium containing 10% FBS, penicillin, and streptomycin in a cell incubator (5% CO_2 and 37 °C). The MTT assay involved seeding 1×10^4 cells (in 100 µL of growth medium in a 96-well plate) were treated by the concentrations (0, 0.6, 3, 6, 7, 12, 25, 50 and 100 µM) of either PTX or SNPs and (0, 0.05, 0.3, 0.6, 1, 2 and 5 µM) of SNPs-PTX@BSA NPs. 10 µL of MTT reagent (5 mg/mL) was added to each well, and the samples were then incubated in the dark (37 °C and 2 h). The cells were then lysed, and formazan crystals were dissolved in 100 µL of DMSO. The absorbance was measured at 570 nm using a microplate reader (BioTek, Power Wave XS). The LD50 concentrations of PTX, SNPs, and SNPs-PTX@BSA were subsequently determined.[33]

Cytomorphological and nuclear morphology changes

MDA-MB-231 cells (5×10^5) were treated with SNPs, PTX, and SNPs-PTX@BSA NPs at LD_{50} concentration and incubated. Following the incubation period, the cells were examined for gross morphological changes using inverted phase-contrast microscopy (Axiovert 2 plus, Zeiss, Germany) using the acridine orange (AO)/ethidium bromide (EB) double staining approach.[34] Briefly, cells were cultured in 6-well plates with overnight incubation. The cells were then treated with SNPs, PTX, and SNPs-PTX@BSA NPs at LD_{50} concentration. Following harvest and washing twice with PBS, the AO/EB solution was added to the cell suspension. The nuclear morphology was evaluated by fluorescence microscopy.

Fluorescent microscopy

The assessment of apoptotic induction (condensation and fragmentation of nucleic DNA) by SNPs-PTX@BSA NPs, DAPI staining, and a DNA-specific dye, using the DOE model, was utilized.[35] The cells (1×10^4) were seeded in 100 µL complete medium in a 96-well plate. Following 24 h of treatment and removing media, the cells were washed (PBS) and fixed in 4% paraformaldehyde (PFA) for 10 min. Finally, the cells were permeabilized with buffer solution (3% PFA and 0.5% Triton X-100) and stained with 50 µL DAPI at an ultimate concentration (1 µg/mL). After 1 h, cell fragmentation, and nuclei condensation images were captured using a fluorescent microscope.

DNA fragmentation assay

MDA-MB-231 cells (1×10^6) were seeded and treated with LD_{50} of SNPs, PTX, and SNPs-PTX@BSA NPs. The extracted DNA was electrophoresed on a 2% agarose gel (20 min at 100 V). Subsequently, it was stained with EB, and the bands were visualized using an ultraviolet transilluminator (Analytik and Jena GmbH).

Cell apoptosis assay

MDA-MB-231 cells (5×10^5) were seeded in 6-well plates and incubated overnight. They were treated with SNPs, PTX, and SNPs-PTX@BSA NPs at LD_{50} for 24 h. After harvest and washing (PBS), the staining was done according to the manufacturer's procedure (Keygen Biotech Co., Nanjing, China). After the cell incubation (15 min at RT and dark), 200 µL binding buffer (BB) containing Annexin V-PE (10 µL) and AAD (5 µL) was added. After that, 300 µL of BB was added to each sample, and the cells were placed on ice. An argon ion laser operating at a 488 nm wavelength was employed for excitation. PE fluorescence was detected in FL-1 using a 525/30 BP filter. In contrast, 7-AAD fluorescence was detected in FL-2 using a 575/30 BP filter. Data analyses were conducted using the FACSDiva software from BD Biosciences Co. (Franklin Lakes, New Jersey, USA).

Cell cycle analysis

MDA-MB-231 cells (5×10^5) were cultured in six-well plates overnight. Then, they were treated with SNPs, PTX, and SNPs-PTX@BSA NPs at LD_{50} concentration for 24 h. Next, the cells were harvested through trypsinization and centrifuged at 2000 rpm (5 min at 4 °C). After being washed twice with ice-cold PBS and fixed with 70% cold ethanol, the cells were incubated on ice for 1 h. The cells were then exposed to 5 µL of ribonuclease solution (10 mg/mL) and stained with 10 µL PI (1 mg/mL) for 30 min at 37 °C in the dark. The DNA content of cells was assessed through flow cytometry, and the percentage of cells in each cell cycle phase was analyzed using BD FACS Comp™ software.

Results and Discussion

Spectroscopic characterization of SNPs and SNPs-PTX@BSANPs

UV-Vis spectroscopy using a Cary 100 Bio instrument (Varian, Australia) showed a broad peak around 430 nm, confirming the formation of SNPs[24,25] and their colloidal dispersion.[36] TEM and SEM images revealed that the SNPs were found to be spherical and sized at less than 20 nm. This observation aligns with the particle-size distribution obtained through DLS analysis (Plus PALS 90, Brookhaven, USA), revealing that SNPs ranged in size from 4.1 to 7.7 nm with a mean diameter of 4.6 nm.

Then, optimization of the synthesized SNPs-PTX@BSA NPs was performed, and this is based on the hydrodynamic size of the NPs. The fate of NPs within the body largely depends on their size. Common barriers to the effective delivery of NPs, especially those sized between 10 nm, include their entry into lymphatic

capillaries following interstitial injection, phagocytosis in lymph nodes, and rapid renal clearance. These factors can hinder the ability of NPs to effectively reach cancer cells and solid tumors.[37-39] Tumor micro-vessels typically have pore sizes ranging from 120 to 1200 nm in diameter,[40,41] enabling particles smaller than 100 nm to extravasate into the tumor tissue through these openings.

The probability of extravasation decreases as particle size increases, particularly for particles larger than 100 nm. In contrast, SNPs-PTX@BSA NPs ranging from 10 to 250 nm can facilitate extravasation into tumor tissue while minimizing uptake by normal tissues, even without opsonization. Therefore, optimizing the size, the 50 nm SNPs-PTX@BSA NPs, which exhibit a uniform spherical morphology, are expected to enhance extravasation and transvascular transport to leaky tumor microvasculature via the enhanced permeability and retention (EPR) effect.[16]

The magnitude of the ZP may influence the optimization process. Negatively charged particles may prevent the aggregation of the NPs. On the other hand, positively charged particles enhance their binding to negatively charged opsonin molecules, resulting in their clearance from the bloodstream.[40,41] Hence, a study that provided BSA-coated PTX nanoemulsion with a ZP of -31 mV,[39] SNPs-PTX@BSA NPs with higher ZP (-53 mV) will be further stabilized. This difference between Abraxane and SNPs-PTX@BSA NPs can be due to SNPs in SNPs-PTX@BSA NPs because the surface charge of SNPs individually is -10 mV. Therefore, the presence of SNPs in SNPs-PTX@BSA NPs makes them more stable. The UV-Vis, fluorescent, and circular dichroism (CD) were conducted with a sample concentration of 40 mM in PBS (0.1 M, pH 7.4).

Furthermore, as shown in Figure 1A, the native BSA absorption peak is presented at 280 nm, attributed to the phenyl group of tryptophan (Trp) and tyrosine (Tyr) residues.[42] Two peaks at 208 nm and 230 nm (Figure 1A, bold dashed line) depict PTX. The UV-Vis analysis of SNPs in PBS indicates the silver surface plasmon position at λ_{max} around 420 nm (Figure 1A dotted line). A comparison of the absorption spectra of naked SNPs and PTX with SNPs-PTX@BSA NPs revealed that the absorbance intensity of SNPs and PTX was reduced. This may be ascribed to the increasing compactness of SNPs and PTX and the change of their microenvironment so that the value of the extinction coefficient of the surface plasmon peak is reduced.

The fluorescence spectrum (Cary Eclipse, Varian, CA, USA) obtained upon excitation at 295 nm provides valuable insights into the molecular environment surrounding the Trp residue.[43] Figure 1B illustrates the emission spectra of BSA and SNPs-PTX@BSA NPs when excited at 295 nm. The results displayed a decrease in fluorescence intensity, likely attributed to the burial of the Trp residue.

Figure 1C indicates that SNPs-PTX@BSA NPs vary in size from 45 to 75 nm (mean particle size 50 nm and PDI 0.4). According to the literature, the effective Z-average diameters of BSA, PTX, and SNPs are 7.2,[44] 11,[45] and 4.6 nm,[19] respectively. Therefore, it can be assumed that SNPs-PTX@BSA NP species form clusters with a diameter of around 50 nm.

Far- and near-CD spectroscopic analyses (Aviv model 215, Lakewood, NJ, USA) confirmed structural alterations in BSA during the preparation of the NPs, using a sample concentration of 40 mM in PBS (0.1 M, pH 7.4). This suggests that Gp60 mediates BSA transcytosis[46] and can potentially be used to treat cancer cells. Additionally, CD spectroscopy examined the conformational changes in BSA during the synthesis of the NPs. The far-UV CD spectrum shows that the overall peak of the α-helix structure in native BSA is similar to that observed in SNPs-PTX@BSA NPs (Figure 1D).[47] This descriptive interpretation was confirmed through spectral deconvolution using the convolutional-deconvolutional neural network (CDNN) software (version 2). The findings show a 1% increase in β-strand content and a 3% decrease in α-helix content when the protein is encapsulated in NP assemblies, as indicated in the inset table of Figure 1D. Therefore, during the fabrication of SNPs-PTX@BSA NPs, the BSA structure is expected to remain largely unchanged, with stability predicted to be around 96%. Tertiary structural alterations were assessed using near-UV CD spectroscopy in the 250-320 nm range. Figure 1E illustrates a characteristic CD spectrum of BSA, consistent with the spectrum reported.[32] It can be observed from Figure 1E that this spectrum remains unchanged, mainly in SNPs-PTX@BSA NPs.

A distinctive peak at 255-265 nm in the CD spectrum, indicative of the BSA tertiary structure, is observed. This unique feature is present in both native BSA and SNPs-PTX@BSA, suggesting minimal changes in the tertiary interactions involving Tyr and Trp residues. However, the molar ellipticity of SNPs-PTX@BSA NPs showed a slight increase after high-pressure homogenization, indicating a minor unfolding of the BSA tertiary structure.

TEM images of negatively stained SNPs-PTX@BSA NPs (Figure 1F and 1G) revealed a spherical shape of SNPs-PTX@BSA NPs with relatively smooth borders and uniform particle size, even though they were all around 50 nm. Due to their metallic condensed nature, SNPs are seen as black spots. However, the PTX and the BSA protein coated around them were relatively transparent. The ZP of SNPs-PTX@BSA NPs is -53 mV, indicating the degree of electrostatic repulsion between adjacent charged clusters. The high ZP value helps stabilize the NPs and prevents them from electrostatically aggregating.[33] The ZP of the BSA NPs and SNPs-PTX@BSA NPs were measured at -7 mV, and -10 mV, respectively.

Dose dependency and cytotoxicity effect

The cell viability assay is a critical procedure in toxicology analysis as it elucidates the cellular response to toxic substances. This assay offers insights into cell death,

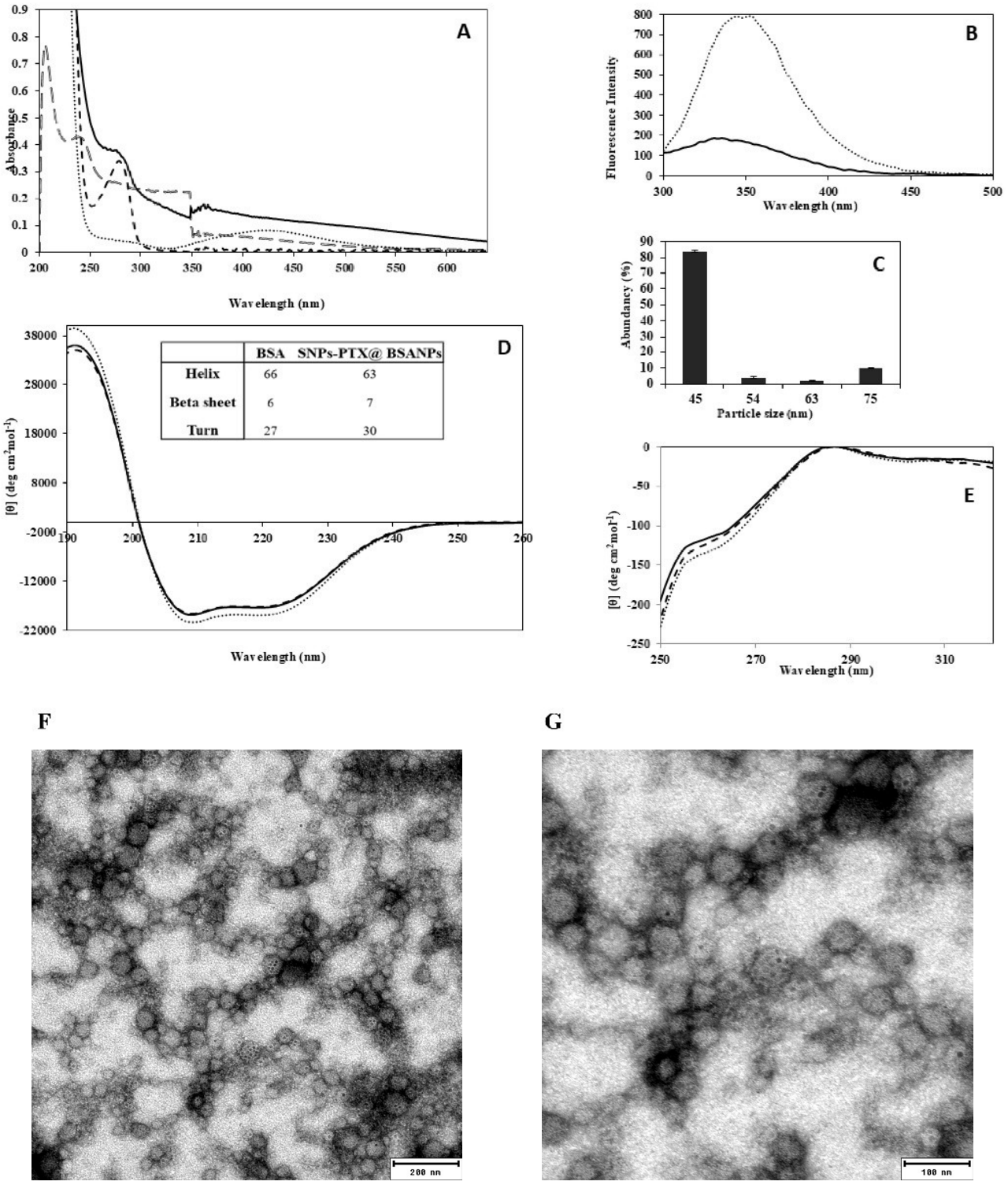

Figure 1. UV-Vis (A), Fluorescence (B), DLS: Particle-size distribution histogram with the PDI 0.4 (C), and CD spectroscopy; far-UV (D), near-UV and (E) including spectra of SNPs-PTX@BSA NPs (solid line), BSA (dotted line), SNPs (dashed line) and PTX (bold dashed line). The table inserted in graph D shows the percentage of secondary structural components of BSA and SNPs-PTX@BSA NPs. The negatively stained SNPs-PTX@BSA NPs (F and G) at different scales (200 and 100 nm)

survival, and metabolic activities, providing valuable information for toxicological studies. In Figure 2, the cytotoxic effect of SNPs was compared with the PTX-induced apoptotic response for MDA-MB-231 cells. As indicated, the cell line shows the pattern of dose-dependent responses for SNPs and PTX, while PTX showed a more significant cytotoxic effect than SNPs. PTX has shown excellent efficacy for BC as a monotherapy or in combination with other cytotoxic drugs like Gefitinib. As shown in Figure 2, the LD_{50} of PTX was obtained to be 3 μM, which agrees with the data reported from PTX in combination with Gefitinib. They showed that the LD_{50}

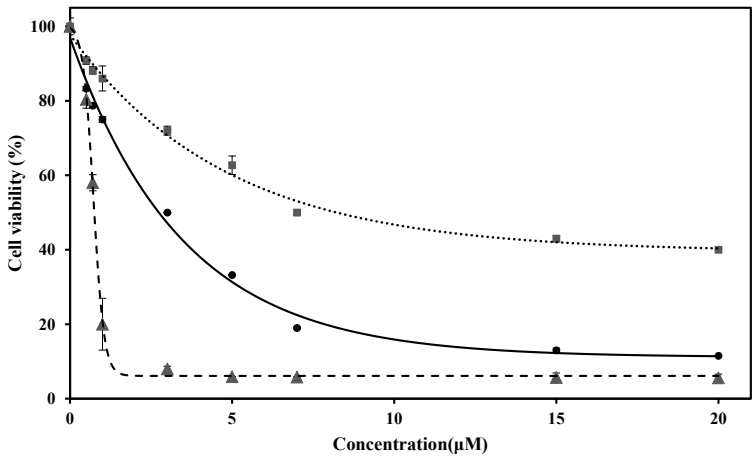

Figure 2. Cell viability of MDA-MB-231 treated with SNPs (dotted line), PTX (solid line), and SNPs-PTX@BSA NPs (dashed line) for 24 h

of PTX against the human BC cells of MDA-MB-231 was 3 ± 0.3 µM.[48]

On the other hand, LD_{50} of SNPs against MDA-MB-231 was 7 µM (Figure 2, dotted line). SNPs (LD_{50} 4 µg/mL) induced a dose-dependent cytotoxicity in human (Chang) liver cells.[28,49] The study showed that SNPs damage the cellular components via the induction of ROS and intracellular suppression of reduced glutathione (GSH). This leads to apoptosis through pathways dependent on mitochondria and caspases, mediated by JNK. The treated cells with SNPs exhibited reduced metabolic activity, with this effect varying depending on the cell type and the size of the NPs.[50] It was also reported that SNPs at higher concentrations than 20 µg/mL, and in the size range from 10 to 50 nm, show cytotoxicity against MCF-7 BC cells after 24 h.[51] Based on the data provided, it can be concluded that PTX exhibits greater cytotoxicity than SNPs. Finally, Figure 2 indicates SNPs, PTX, and SNPs-PTX@BSANPs induced dose-dependent cytotoxicity on MDA-MB-231 with LD_{50} of 0.64, 0.11, and 0.75 µM, respectively.

Combination of PTX and SNPs

The statistical design with different ratios of PTX and SNPs for the combination treatment was carried out using RSM (Table S1). To obtain the best concentration of SNPs and PTX in co-treatment, the experimental results of RSM (Table S1B) were analyzed by Design Expert Software.

The concentrations of 1.03 µM for PTX and 5.75 µM for SNPs were selected as the best co-treatment concentration, leading to 50% cytotoxicity in MDA-MB-231 cells. As seen in Figures S1 and S2, the higher ratio of PTX:SNPs exhibited a superior cytotoxic effect. In contrast, the lower ratio of PTX:SNPs exhibited lower toxicity than 50%. The LD_{50} value of the co-treatment was notably lower than that of the individual treatments, suggesting a synergistic effect in the co-treatment process.

Anticancer effect of SNPs-PTX@BSA NPs

We have already shown that coating SNPs with BSA, improves the anticancer effect, cell uptake, and release profile of SNPs.[18] It has already been reported that BSA coating increases the anticancer effect of PTX remarkably.[39,52-54] Therefore, based on these experiences, SNPs-PTX@ BSA NPs were designed. The SNPs-PTX@ BSA NPs formulation was prepared using a modified nanoprecipitation technique. To synthesize the SNPs-PTX@BSA NPs, the ratio (PTX:SNPs) was selected based on the data reported in Table S1D. The concentration of BSA, the ratio of BSA to anticancer agents, and pH were regarded as influential factors in optimizing the SNPs-PTX@BSA NPs preparation (Table S2). RSM designed optimization as a statistical design of the experiment. Then, the data was analyzed using Design Expert software.

As seen in Table S2, the best-obtained size for SNPs-PTX@BSA NPs was 50 nm (containing 1.42% of BSA), which is big enough to evade opsonization and small enough to extravasate into tumor tissue. As shown in Figure S3 and S4, increasing the BSA concentration resulted in larger SNPs-PTX@BSA NPs. This finding has also been confirmed by other studies for PTX@BSA NPs.[38,39]

The studies showed that increasing the BSA concentration (1-4%) led to larger BSA NPs with decreased ZP. Because BSA is a negatively charged molecule, raising the BSA amount in the initial solution encourages the creation of more intermolecular disulfide bonds. This process induces protein aggregation, resulting in the formation of larger SNPs-PTX@BSA NPs. The optimum ratio of BSA to anticancer agents was 6.43. The particle size is mainly controlled by the initial anticancer agents in the emulsion. A decrease in the anticancer agent concentration will decrease the final particle size.[55] This finding supports the results represented in Figure S3 and S4.

Apoptosis induction

The cells were treated with SNPs, PTX, and SNPs-PTX@ BSA NPs at their LD_{50} concentrations to explore the cell death mechanism. After 24 h treatment, the cells were

investigated using an inverted confocal microscope, AO/EB staining approach, and DNA fragmentation assay. Figure 3 A-D, indicate s the morphological alteration in MDA-MB-231 cells induced by SNPs-PTX@BSA NPs, PTX, and SNPs, compared with untreated cells. Cell growth inhibition, cytoplasmic condensation, creation of curved forms, loss of membrane integrity, and apoptotic bodies were observed in the cells treated with SNPs-PTX@BSA NPs. However, these alterations were not observed in the treated cells (PTX and SNPs) or the untreated cells. These observations indicate that SNPs-PTX@BSA NPs induce cell death, whereas the treated cells (PTX and SNPs), and non-treated cells remained active. Consequently, 0.11 µM PTX and 0.64 µM SNPs did not show distinguishable morphological changes individually, but when they were embedded in SNPs-PTX@BSANPs, synergistically, they affected the cell morphology.

The AO/EB staining method was employed to observe nuclei alterations indicative of apoptosis. In Figure 4, a fluorescence microscope contrasts the stained treated cells with the control cells. The orange spots correspond to the nuclei of apoptotic cells (Figure 4D), while the green spots represent viable cells.

Approximately 50% of the cells treated with SNPs-PTX@BSANPs displayed orange spots. However, the treated cells by PTX, SNPs, and non-treated cells did not

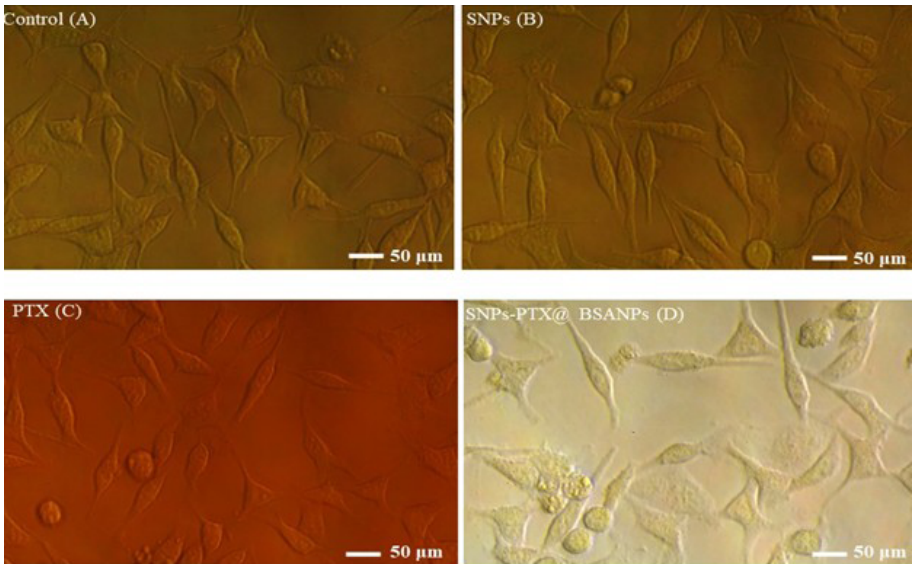

Figure 3. Inverted microscopic images of MDA-MB-231 cells. The normal cells as control (A) are compared with the cells treated with SNPs (B), PTX (C), and SNPs-PTX@BSA NPs (D) for 24 h

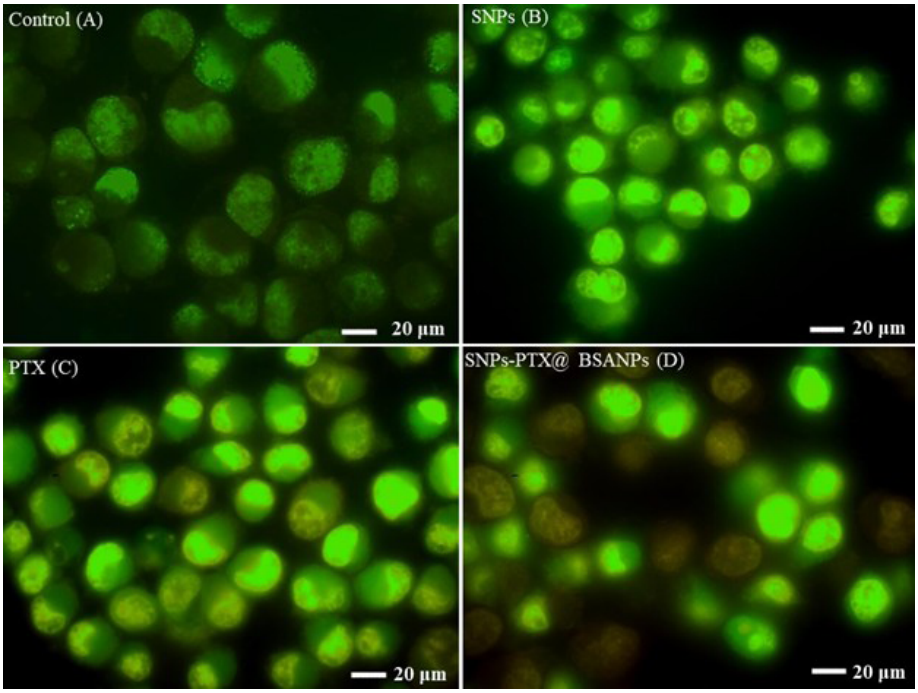

Figure 4. Fluorescent microscopic images of MDA-MB-231 cells stained with a mixture of AO and EB. The control or normal cells indicate (A) the cells treated with SNPs (B), PTX (C), and SNPs-PTX@BSA NPs (D) for 24 h

show significant symptoms of apoptosis in the nuclei. This result verified that the combination of PTX and SNPs with embedding in BSA NPs synergistically increased anticancer properties.

During apoptosis, there is an increase in cell membrane permeability, leading to enhanced uptake of DAPI, resulting in a more intense blue fluorescence.[56] The cells were treated with SNPs, PTX, and SNPs-PTX@BSA NPs. The non-treated cells were also stained by DAPI fluorescent dye (Figure 5). It is shown that only cells treated with SNPs-PTX@BSA NPs displayed apoptosis (cells with bright fluorescence and fragmented nucleus).

In contrast, the cells treated with PTX, SNPs, or non-treated cells presented no apoptosis. It suggests that 0.75 µM SNPs-PTX@BSA NPs induce cell apoptosis and DNA fragmentation. However, the cells treated with 0.11 µM PTX and 0.64 µM SNPs or non-treated cells did not exhibit bright fluorescence and a fragmented nucleus. This is another document on this claim that verified the combination of PTX and SNPs with embedding in BSANPs synergistically increased apoptotic properties.

A necessary confirmation of the activation of the apoptosis pathway was the detection of the DNA ladder fragmentation pattern, which results from endonuclease cleavage during apoptosis.[57] The DNA of MDA-MB-231 cells treated with LD_{50} concentrations of SNPs-PTX@BSA NPs was extracted and checked from horizontal agarose gel electrophoresis (GE) (agarose 1.5%, 70 V, 20 min). The results of the DNA "laddering" pattern (extracted from the cells) treated with SNPs-PTX@BSA NPs, PTX, and SNPs, are shown in Figure 6. The DNA ladder fragmentation pattern was only present in cells treated with SNPs-PTX@BSA NPs.

The quantification of the apoptosis stage with SNP, PTX, and SNPs-PTX@BSA NPs-treated cells was conducted by flow cytometry using Annexin V-PE and 7-AAD staining dyes. Early apoptosis was identified using Annexin V-PE, which attaches to externalized phosphatidyl serine (PS) ligands on apoptotic cell surfaces. 7-AAD fluorescent dye, which recognizes early apoptosis, can only enter dead and damaged cells through the disrupted membrane. Figure 7 shows the SNPs-PTX@BSA NPs induced apoptosis in the cells after 24 h of treatment at LD_{50}. However, mortality occurrence in PTX and SNPs-treated cells was negligible.

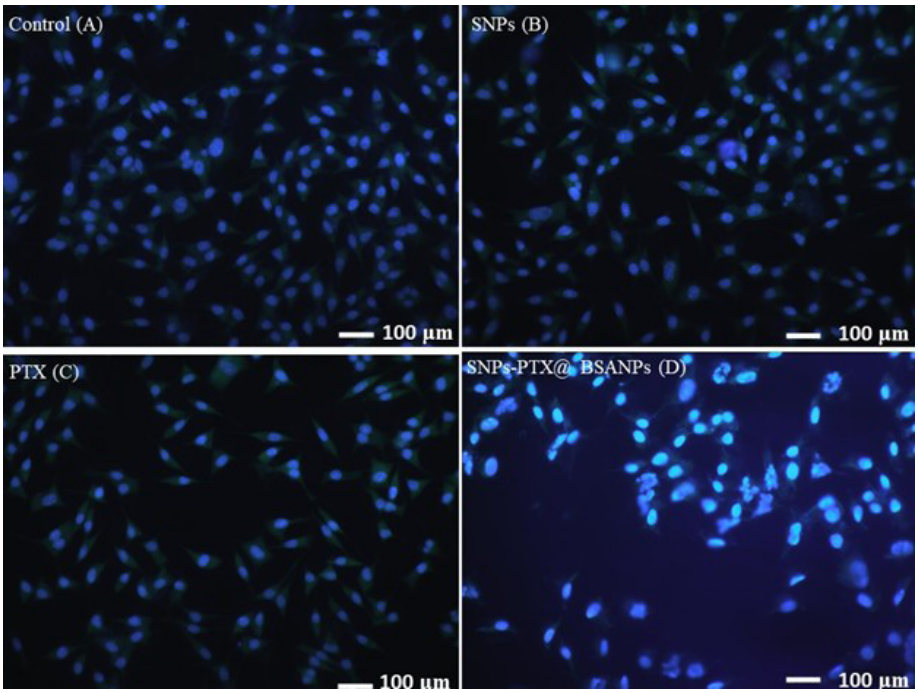

Figure 5. Fluorescent microscopic images of DAPI stained MDA-MB-231 cells treated with SNPs (B) PTX (C) and SNPs-PTX@BSA NPs (D). The untreated cells were used as control (A) for 24 h

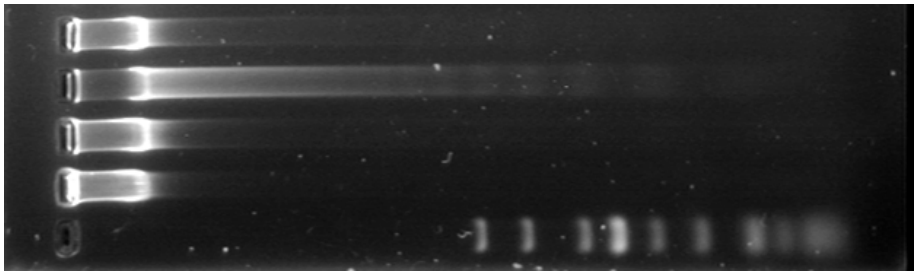

Figure 6. GE of DNA extracted from MDA-MB-231 cells. Lane A: 1 kB ladder, Lane B: Untreated cells (control), Lanes C, D, and E sand for treatment of the cells with SNPs, PTX, and SNPs-PTX@BSA NPs, respectively 24 h

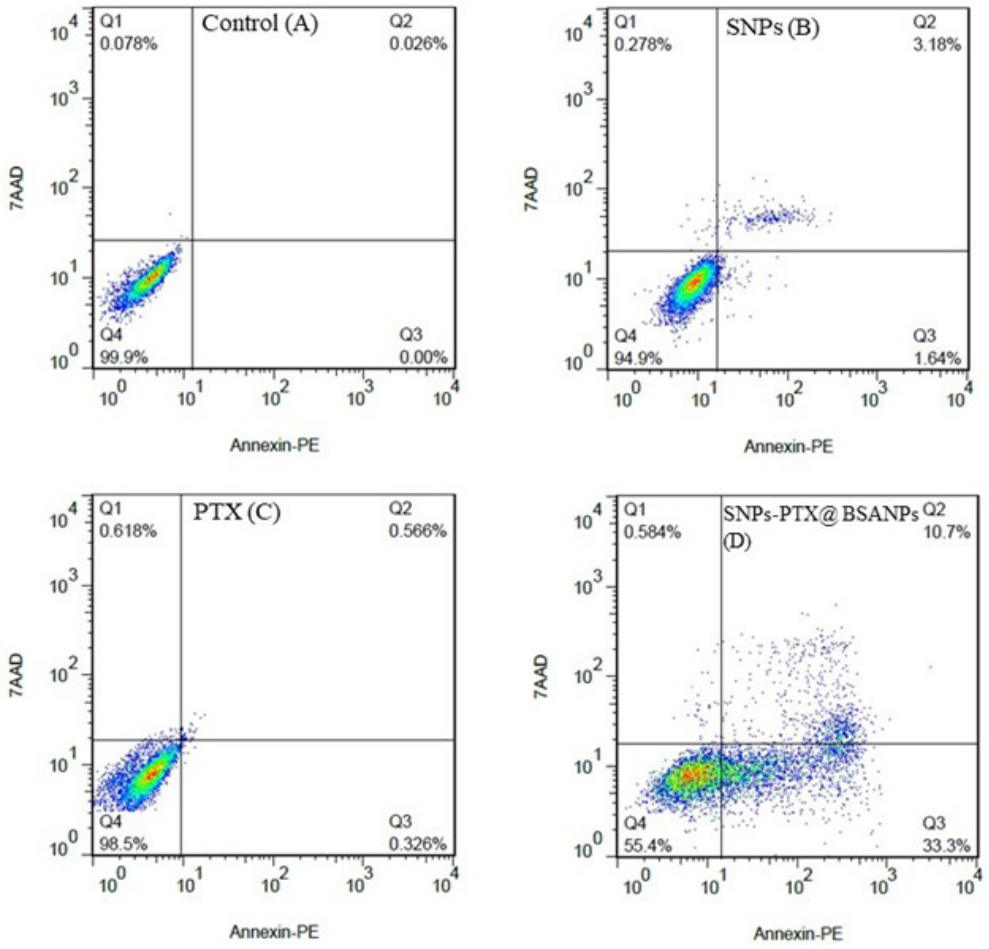

Figure 7. Two-dimensional contour density plots by flow cytometry. Figures A-D depict treated cells with SNPs, PTX, and SNPs-PTX@BSA NPs, respectively (Vs the control). Cell necrosis and apoptosis levels were assessed using Annexin V-PE and 7-AAD dyes for 24 h

Results of inverted microscopic images, AO/EB and DAPI staining methods, DNA fragmentation assay, and flow cytometry confirmed that apoptosis is the mechanism of cell death following treatment with SNPs-PTX@BSA NPs. Since symptoms of apoptosis in all four other tests in the treated cells by 0.11 µM PTX and 0.64 µM SNPs, which exist in SNPs-PTX@BSA NPs were not significant. Therefore, it can be concluded that co-treatment of PTX and SNPs with embedding in BSANPs synergistically induces apoptotic properties. SNPs-PTX@BSA NPs, when compared to PTX and SNPs used individually, maybe a more compelling candidate for chemotherapy due to the lower concentration required of each agent when combined.

Cell cycle analysis

The cell cycle evaluation investigated the cytotoxic potential of each SNPs, PTX, and their combination SNPs-PTX@BSA NPs on MDA-MB-231 cells. PTX attaches to the α,β-tubulin dimer located within the microtubules. Hence, exposing a cell to the LD_{50} concentration of PTX results in G2/M arrest in rapidly dividing cells, ultimately triggering apoptosis. However, the treatment of cells at LD_{50} concentrations of SNP induces cell cycle arrest at the S/G2/M phase due to DNA damage and improper DNA repair.[58] Figure 8 indicates the S/G2/M phase arrest and the presence of a subG1 cell population induced by SNPs-PTX@BSA NPs. Treatment with PTX (0.11 µM) led to 7.72% of cells being in the subG1 phase with negligible changes in cell cycle phases. In support of our data, other researchers have shown that low concentrations of PTX cause subG1 cell populations to be without G1 arrest and cell prevention from passing through the S phase and entering mitosis.[59,60] Demidenko et al[46] argued that a subG1 peak in cells treated with low concentrations of PTX exists because of prolonged mitosis. However, the cells continue to divide, resulting in the production of either two cells or three cells (tripolar mitosis). In the subG1 stage, the cells display viable and non-apoptotic forms. Certain cells fused back together and then proceeded to mitosis, frequently resulting in three cells before being arrested in the following cell-cycle interphase.[59,60]

On the other hand, treatment with 0.64 µM SNPs resulted in no significant changes in cell cycle phases. The cocktail of PTX and SNPs with embedding in BSANPs induced a subG1 cell population (7.97%), which was slightly higher than PTX-treated cells (7.72%) as single drugs. In contrast to PTX, SNPs-PTX@BSA NPs induced 31% S and 26% G_2/M cell population, significantly higher than treatment with PTX (0.11 µM) and SNPs (0.64 µM).

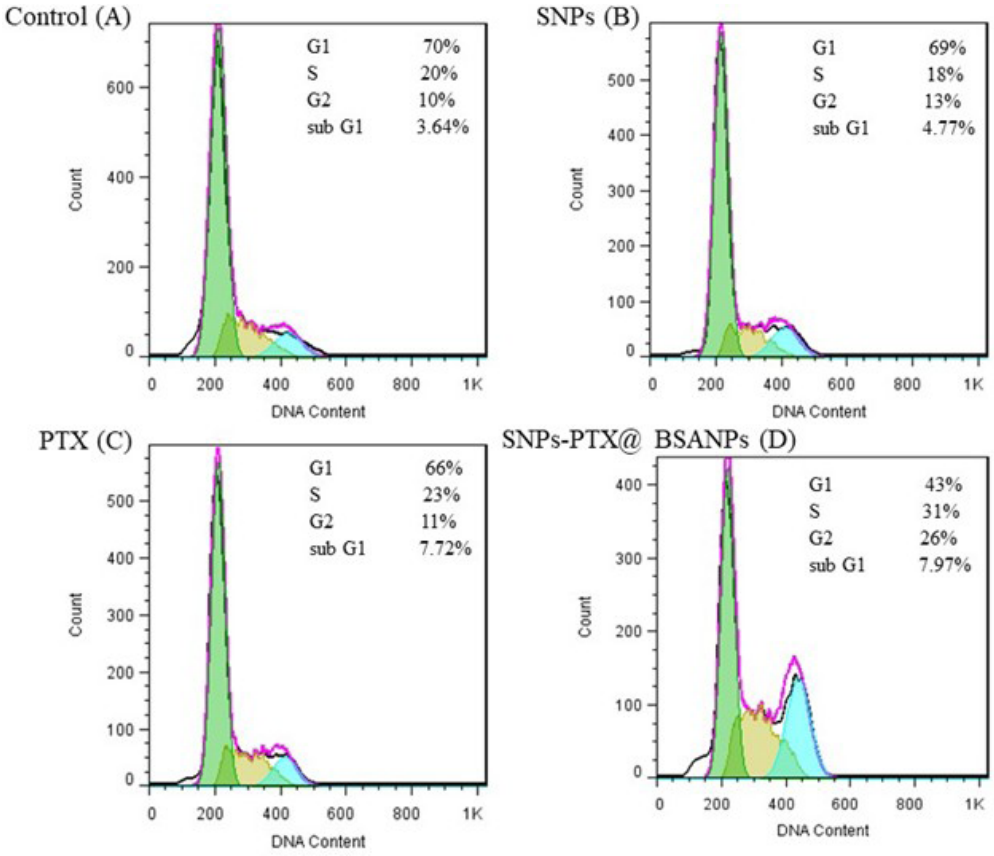

Figure 8. Flow cytometry analysis of the cell cycle profile through treatment of A) control B) SNPs C) PTX to, and D) SNPs-PTX@BSA NPs for 24 h

Formation and toxicity mechanism of SNPs-PTX@ BSANPs

The severe side effects of anticancer drugs limit their dosages, impacting chemotherapy efficacy. Exposure to both normal and cancer cells is the key limitation. Successful cancer treatments rely on targeting rapidly dividing cancer cells for selective destruction.[61,62] To address this issue, various combinations of anticancer drugs have been explored to improve the efficacy of tumor chemotherapy.[61,63] Due to each chemotherapeutic agent's distinct mechanisms and side effects, each drug has an upper concentration limit to inhibit cancer cell growth while reducing harm to normal cells. Therefore, selecting the appropriate combination of chemotherapeutic agents can optimize treatment effectiveness and minimize adverse effects.[64-66]

The experimental findings demonstrated that combining drugs enhanced chemotherapeutic effectiveness compared to using single drugs. PTX, a commonly utilized anticancer chemotherapy, attaches to the β-subunit of tubulin, causing stability induction in microtubule function and mitosis. A high dose of PTX can harm both normal and cancer cells, while a low dose of SNPs enhances cell sensitivity to PTX, promoting cell death and improving anticancer outcomes. The synergy between PTX and SNPs is likely due to silver ions' cytotoxic impact on tumor cells through ROS generation, complementing the anti-proliferative properties of PTX.[67-69]

The formation mechanism of SNPs-PTX@BSANPs involves the encapsulation of SNPs and PTX within the BSA matrix, stabilized by intermolecular thiol-silver-thiol bonds between cysteine residues of BSA molecules. This encapsulation is supported by the high affinity of PTX for albumin and the relative sizes of the components involved. Our earlier publication delves into four of these scenarios extensively.[70] The beginning of these scenarios is the formation of superoxide radicals and ions due to the application of ultrasonic force and the increase of pressure and temperature at a point in the solvent. Superoxide attacks BSA by disrupting existing disulfide bonds between cysteine residues of each BSA and the production of cysteinyl radicals. Given the high probability of SNPs and PTX being buried inside the BSA NPs, the encapsulation mechanism ensures that these components are effectively integrated within the BSA matrix, enhancing the stability and functionality of the NPs.

Ultrasonication removes the citrate layer on SNPs, leading to silver oxidation by citrate ions. With ultrasonic forces, silver ions break disulfide bonds to create cysteinyl radicals. Certain cysteinyl radicals are inhibited from converting into SH groups within the cysteine residues of BSA molecules. In the initial pathway, thiol cysteine free radicals are oxidized with peripheral electrons and protons, resulting in free SH groups. The second possibility is that by joining two cysteinyl radicals, the intramolecular disulfide bonds could be reformed

between cysteine residues of each BSA. In the second pathway, thiol cysteine radicals can create intramolecular bonds and attach to other cysteines in albumin. In the third pathway, cysteines from separate albumin molecules form intermolecular bonds. These NPs do not contain PTX or SNPs. Due to the intense attraction between cysteinyl radicals and silver ions, some cysteinyl radicals from neighboring BSA molecules may connect through a silver bridge (thiol-silver-thiol). This means that in the fourth pathway, SNPs@BSA are formed (Figure 9). This theory aligns with findings from other studies.[62,63] BSA can interact with heavy metals like silver because of the BSA thiol functional group, and the interaction can disrupt disulfide bonds and cause protein denaturation.[71] A cryo-TEM image of PTX@BSANPs reveals that PTX is attached to BSA through non-covalent hydrophobic interactions and is surrounded by a layer of BSA crosslinked to a certain extent.[54,72] A prior X-ray powder diffraction analysis has shown that PTX inside the NPs is amorphous and lacks a crystalline structure.[73] This finding suggests that PTX is likely located within the core of the nano-composite through hydrophobic interactions rather than covalent bonding. The presence of PTX in the reaction creates a hydrophobic cavity due to ultrasonic force application, supporting arguments from a recent study.[66] The sixth pathway involves the creation of thiol-silver-thiol bonds in the presence of SNPs, resulting in the development of a hydrophobic cavity containing PTX. This process leads to SNPs-PTX@BSANPs, as illustrated in Figure 9.

Toxicity of SNPs-PTX@BSA NPs against MDA-MB-231 cells was 27 times higher than that of PTX (LD_{50} 3 μM) alone and roughly 11 times higher than that of SNPs (LD_{50} 7 μM) alone in the treatment. The LD_{50} value of SNPs-PTX@BSANPs is notably lower than that of each drug, indicating that co-delivery of PTX and SNPs with BSANPs enhances chemotherapeutic effectiveness compared to single drug treatments.[46] Moreover, the BSA uptake also increases due to the higher metabolism rate of cancer cells.[74] Hence, BSA multiplies the synergistic anticancer efficacy of PTX and SNPs.

Given the absence of apoptosis symptoms in cells treated with 0.11 μM PTX and 0.64 μM SNPs, which are components of SNPs-PTX@BSA NPs, we propose that the combined administration of PTX and SNPs encapsulated in BSANPs synergistically induces apoptotic characteristics. SNPs-PTX@BSA NPs triggered substantial apoptosis (both early and late stages) and led to a cell cycle arrest at the S/G2/M phase, accompanied by a rise in the subG1 population. The elevated G2/M phase arrest suggests suppression of cell division and proliferation,[75] probably due to PTX binding to tubulin and increased S phase arrest, which could be derived from DNA damage caused by SNPs. The quantitative results confirm that the apoptotic effect of SNPs-PTX@BSANPs is due to the synergistic interaction (between PTX and SNPs) within the BSANPs.

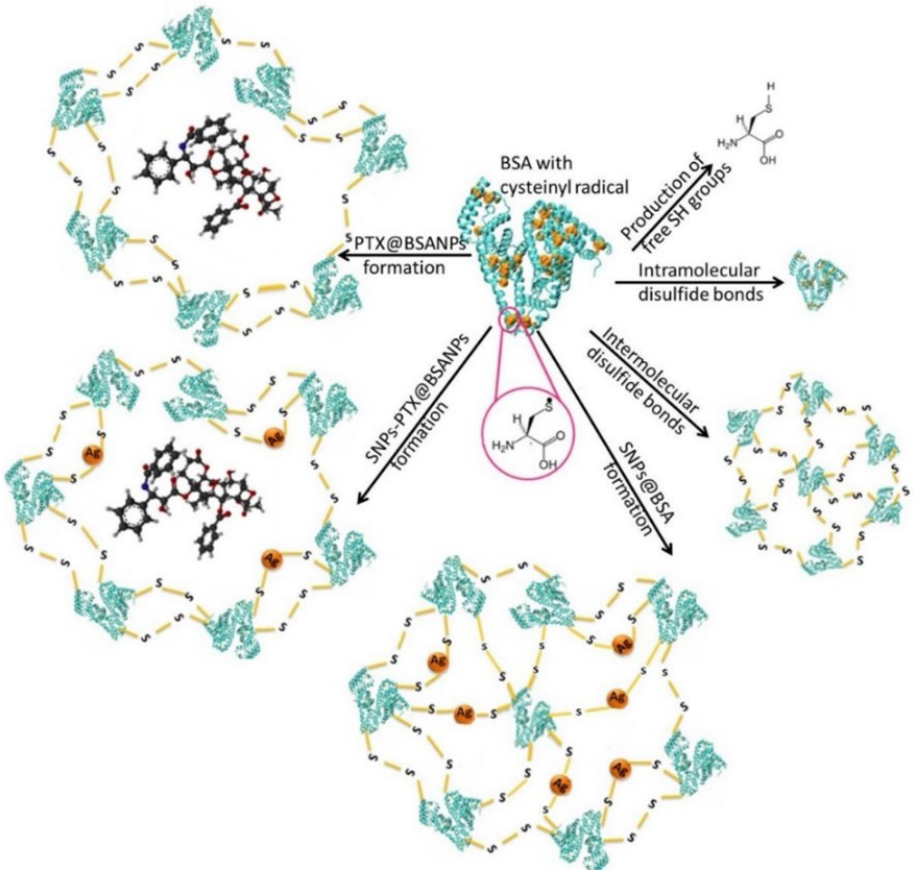

Figure 9. Schematic representation of the various reaction paths for the proposed mechanisms for the formation of SNPs-PTX@BSANPs

The toxicity mechanism of SNPs-PTX@BSA NPs entails mitochondrial apoptotic induction by both SNPs and PTX. It is postulated that following internalization of SNPs-PTX@BSA NPs mediated by specific BSA-binding receptors, BSA dissociates from SNPs and PTX.

BSA re-enters circulation through the lymphatic system, while internalized SNPs disrupt mitochondrial function, triggering ROS production. ROS and silver ions released from SNPs induce DNA damage by crossing the nuclear membrane. This damage can lead to chromosomal abnormalities, cell cycle arrest in the S/G2 phase, and apoptosis. In parallel, PTX binds to microtubules, halting the cell cycle in the G2 phase and inducing cell death via a caspase-independent apoptotic pathway.

Alternatively, mitochondrial activation through death receptor-independent cytoplasmic signals releases cytochrome C and the formation of the apoptosome, comprising cytochrome C, ATP, APAF-1, and procaspase-9. This apoptosome formation initiates caspase-9 activation, activating effector caspase-3 and subsequent processing and activation of procaspase-8. The processing of caspase-8 can occur through auto-catalysis. Caspase-3 can reactivate mitochondrial apoptosis. The synergistic anticancer effect of SNPs-PTX@BSA NPs is demonstrated by their cellular uptake via BSA receptor-mediated internalization, inducing mitochondrial apoptosis through SNPs and PTX. SNPs increase ROS production, while PTX initiates death receptor-independent cytoplasmic signaling and activates the Caspases-3 and -8 pathways, collectively promoting apoptosis.

Conclusion

The nanoprecipitation method successfully synthesized SNPs-PTX@BSANPs with a size of 50 nm and a surface potential of -56 mV. During this process, BSA encapsulated SNPs and PTX. These NPs were tested for their anticancer efficacy against MDA-MB-231 invasive BC cells (LD50 0.75 μM). Experimental findings indicate that the combined ratio of PTX and SNPs displayed more significant cytotoxicity than the individual drugs. Notably, the NPs loaded with both drugs showed superior cytotoxicity at a significantly lower dose than the cocktail combination. The SNPs-PTX@BSANPs showed enhanced efficacy compared to individual drugs, resulting in accelerated and prolonged apoptosis induction. Moreover, they induced a more potent cell cycle arrest in the S/G2/M phase and increased the subG1 population. The combination of SNPs and PTX within albumin-based NPs improved the efficacy of treatment for BC cells. As a result, we propose that SNPs-PTX@BSA NPs hold promise for in vivo evaluation of the treatment of invasive BC.

Authors' Contribution

Conceptualization: Marzieh Azizi, Hedayatollah Ghourchian, Bo Nyström.
Data curation: Marzieh Azizi, Seyed Hossein Kiaie.
Formal analysis: Marzieh Azizi, Hedayatollah Ghourchian, Seyed Hossein Kiaie, Fatemeh Yazdian.
Funding acquisition: Hedayatollah Ghourchian.
Investigation: Marzieh Azizi, Fatemeh Yazdian, Mohammad Sheibani.
Methodology: Marzieh Azizi, Seyed Hossein Kiaie.
Project administration: Hedayatollah Ghourchian.
Resources: Mohammad Sheibani, Fatemeh Yazdian.
Supervision: Hedayatollah Ghourchian, Bo Nyström.
Writing-original draft: Marzieh Azizi, Seyed Hossein Kiaie.
Writing-review & editing: Marzieh Azizi, Seyed Hossein Kiaie, Mohammad Sheibani.

Competing Interests

The authors declare that they have no known competing financial interests or personal relationships that could have appeared to influence the work reported in this paper.

Consent for Publication

Not applicable.

Data Availability Statement

The data supporting this study's findings are available from the corresponding and first author upon reasonable request.

Funding

This study was funded by University of Tehran, Iran.

Supplementary Files

Supplementary file 1 contains Tables S1-S2 and Figures S1-S4 .

References

1. Hofmann M, Guschel M, Bernd A, Bereiter-Hahn J, Kaufmann R, Tandi C, et al. Lowering of tumor interstitial fluid pressure reduces tumor cell proliferation in a xenograft tumor model. Neoplasia. 2006;8(2):89-95. doi: 10.1593/neo.05469.
2. Szakács G, Paterson JK, Ludwig JA, Booth-Genthe C, Gottesman MM. Targeting multidrug resistance in cancer. Nat Rev Drug Discov. 2006;5(3):219-34. doi: 10.1038/nrd1984.
3. Shapira A, Livney YD, Broxterman HJ, Assaraf YG. Nanomedicine for targeted cancer therapy: towards the overcoming of drug resistance. Drug Resist Updat. 2011;14(3):150-63. doi: 10.1016/j.drup.2011.01.003.
4. Sreekanth CN, Bava SV, Sreekumar E, Anto RJ. Molecular evidences for the chemosensitizing efficacy of liposomal curcumin in paclitaxel chemotherapy in mouse models of cervical cancer. Oncogene. 2011;30(28):3139-52. doi: 10.1038/onc.2011.23.
5. Borg AG, Burgess R, Green LM, Scheper RJ, Yin JA. Overexpression of lung-resistance protein and increased P-glycoprotein function in acute myeloid leukaemia cells predict a poor response to chemotherapy and reduced patient survival. Br J Haematol. 1998;103(4):1083-91. doi: 10.1046/j.1365-2141.1998.01111.x.
6. Gregorcyk S, Kang Y, Brandt D, Kolm P, Singer G, Perry RR. Best clinical research paper P-glycoprotein expression as a predictor of breast cancer recurrence. Eur J Surg Oncol. 1996;22(1):121. doi: 10.1016/s0748-7983(96)92045-4.
7. Burger H, Foekens JA, Look MP, Meijer-van Gelder ME, Klijn JG, Wiemer EA, et al. RNA expression of breast cancer resistance protein, lung resistance-related protein, multidrug resistance-associated proteins 1 and 2, and multidrug resistance gene 1 in breast cancer: correlation with chemotherapeutic response. Clin Cancer Res. 2003;9(2):827-36.

8. Materna V, Pleger J, Hoffmann U, Lage H. RNA expression of MDR1/P-glycoprotein, DNA-topoisomerase I, and MRP2 in ovarian carcinoma patients: correlation with chemotherapeutic response. Gynecol Oncol. 2004;94(1):152-60. doi: 10.1016/j.ygyno.2004.03.035.
9. Ramasamy T, Kim J, Choi HG, Yong CS, Kim JO. Novel dual drug-loaded block ionomer complex micelles for enhancing the efficacy of chemotherapy treatments. J Biomed Nanotechnol. 2014;10(7):1304-12. doi: 10.1166/jbn.2014.1821.
10. Min H, Yao J, Allinen M, Cai L, Polyak K. The role of the tumor microenvironment in breast cancer progression. Breast Cancer Res. 2005;7(2):S17. doi: 10.1186/bcr1060.
11. Ji X, Lu Y, Tian H, Meng X, Wei M, Cho WC. Chemoresistance mechanisms of breast cancer and their countermeasures. Biomed Pharmacother. 2019;114:108800. doi: 10.1016/j.biopha.2019.108800.
12. Tufail M, Cui J, Wu C. Breast cancer: molecular mechanisms of underlying resistance and therapeutic approaches. Am J Cancer Res. 2022;12(7):2920-49.
13. Alalawy AI. Key genes and molecular mechanisms related to paclitaxel resistance. Cancer Cell Int. 2024;24(1):244. doi: 10.1186/s12935-024-03415-0.
14. Yusuf RZ, Duan Z, Lamendola DE, Penson RT, Seiden MV. Paclitaxel resistance: molecular mechanisms and pharmacologic manipulation. Curr Cancer Drug Targets. 2003;3(1):1-19. doi: 10.2174/1568009033333754.
15. Li QQ, Cao XX, Xu JD, Chen Q, Wang WJ, Tang F, et al. The role of P-glycoprotein/cellular prion protein interaction in multidrug-resistant breast cancer cells treated with paclitaxel. Cell Mol Life Sci. 2009;66(3):504-15. doi: 10.1007/s00018-008-8548-6.
16. Ramasamy T, Kim JH, Choi JY, Tran TH, Choi HG, Yong CS, et al. pH sensitive polyelectrolyte complex micelles for highly effective combination chemotherapy. J Mater Chem B. 2014;2(37):6324-33. doi: 10.1039/c4tb00867g .
17. Xiao H, Verdier-Pinard P, Fernandez-Fuentes N, Burd B, Angeletti R, Fiser A, et al. Insights into the mechanism of microtubule stabilization by Taxol. Proc Natl Acad Sci U S A. 2006;103(27):10166-73. doi: 10.1073/pnas.0603704103.
18. McGrogan BT, Gilmartin B, Carney DN, McCann A. Taxanes, microtubules and chemoresistant breast cancer. Biochim Biophys Acta. 2008;1785(2):96-132. doi: 10.1016/j.bbcan.2007.10.004.
19. Sugimura M, Sagae S, Ishioka S, Nishioka Y, Tsukada K, Kudo R. Mechanisms of paclitaxel-induced apoptosis in an ovarian cancer cell line and its paclitaxel-resistant clone. Oncology. 2004;66(1):53-61. doi: 10.1159/000076335.
20. Liu R, Chen Y, Liu G, Li C, Song Y, Cao Z, et al. PI3K/AKT pathway as a key link modulates the multidrug resistance of cancers. Cell Death Dis. 2020;11(9):797. doi: 10.1038/s41419-020-02998-6.
21. Hall MD, Martin C, Ferguson DJ, Phillips RM, Hambley TW, Callaghan R. Comparative efficacy of novel platinum(IV) compounds with established chemotherapeutic drugs in solid tumour models. Biochem Pharmacol. 2004;67(1):17-30. doi: 10.1016/j.bcp.2003.07.016.
22. Bagherifar R, Kiaie SH, Hatami Z, Ahmadi A, Sadeghnejad A, Baradaran B, et al. Nanoparticle-mediated synergistic chemoimmunotherapy for tailoring cancer therapy: recent advances and perspectives. J Nanobiotechnology. 2021;19(1):110. doi: 10.1186/s12951-021-00861-0.
23. Ge L, You X, Huang J, Chen Y, Chen L, Zhu Y, et al. Human albumin fragments nanoparticles as PTX carrier for improved anti-cancer efficacy. Front Pharmacol. 2018;9:582. doi: 10.3389/fphar.2018.00582.
24. Sanpui P, Chattopadhyay A, Ghosh SS. Induction of apoptosis in cancer cells at low silver nanoparticle concentrations using chitosan nanocarrier. ACS Appl Mater Interfaces. 2011;3(2):218-28. doi: 10.1021/am100840c.
25. Hsin YH, Chen CF, Huang S, Shih TS, Lai PS, Chueh PJ. The apoptotic effect of nanosilver is mediated by a ROS- and JNK-dependent mechanism involving the mitochondrial pathway in NIH3T3 cells. Toxicol Lett. 2008;179(3):130-9. doi: 10.1016/j.toxlet.2008.04.015.
26. Fan D, Cao Y, Cao M, Wang Y, Cao Y, Gong T. Nanomedicine in cancer therapy. Signal Transduct Target Ther. 2023;8(1):293. doi: 10.1038/s41392-023-01536-y.
27. Heidari Majd M. Combination therapy of cisplatin and green silver nanoparticles enhances cytotoxicity and apoptosis in breast cancer cells. Cancer Plus. 2024;6(1):2770. doi: 10.36922/cp.2770.
28. Tabbasam R, Khursid S, Ishaq Y, Farrukh SY. Synergistic cytotoxic effects of doxorubicin loaded silver, gold and zinc oxide nanoparticles in HepG2 liver cancer cells. Bionanoscience. 2024;15(1):105. doi: 10.1007/s12668-024-01747-9.
29. Zou J, Zhu B, Li Y. Functionalization of silver nanoparticles loaded with paclitaxel-induced A549 cells apoptosis through ROS-mediated signaling pathways. Curr Top Med Chem. 2020;20(2):89-98. doi: 10.2174/1568026619666191019102219.
30. Muhammad N, Zhao H, Song W, Gu M, Li Q, Liu Y, et al. Silver nanoparticles functionalized paclitaxel nanocrystals enhance overall anti-cancer effect on human cancer cells. Nanotechnology. 2021;32(8):085105. doi: 10.1088/1361-6528/abcacb.
31. Azizi M, Ghourchian H, Yazdian F, Dashtestani F. Anticancer and antioxidant properties of Ag NPs coated with BSA NPs. Iran J Chem Eng. 2015;12(1):22-9.
32. Rashid MU, Bhuiyan MK, Quayum ME. Synthesis of silver nano particles (Ag-NPs) and their uses for quantitative analysis of vitamin C tablets. Dhaka Univ J Pharm Sci. 2013;12(1):29-33. doi: 10.3329/dujps.v12i1.16297.
33. Fisher GA, Sikic BI. Clinical studies with modulators of multidrug resistance. Hematol Oncol Clin North Am. 1995;9(2):363-82.
34. Cohen JJ. Apoptosis. Immunol Today. 1993;14(3):126-30. doi: 10.1016/0167-5699(93)90214-6.
35. Lewandowska U, Szewczyk K, Owczarek K, Hrabec Z, Podsędek A, Koziołkiewicz M, et al. Flavanols from Japanese quince (*Chaenomeles japonica*) fruit inhibit human prostate and breast cancer cell line invasiveness and cause favorable changes in Bax/Bcl-2 mRNA ratio. Nutr Cancer. 2013;65(2):273-85. doi: 10.1080/01635581.2013.749292.
36. Das VK, Harsh SN, Karak N. Highly efficient and active silver nanoparticle catalyzed conversion of aldehydes into nitriles: a greener, convenient, and versatile 'NOSE' approach. Tetrahedron Lett. 2016;57(5):549-53. doi: 10.1016/j.tetlet.2015.12.083.
37. Wang J, Lu Z, Gao Y, Wientjes MG, Au JL. Improving delivery and efficacy of nanomedicines in solid tumors: role of tumor priming. Nanomedicine (Lond). 2011;6(9):1605-20. doi: 10.2217/nnm.11.141.
38. Lomis N, Westfall S, Farahdel L, Malhotra M, Shum-Tim D, Prakash S. Human serum albumin nanoparticles for use in cancer drug delivery: process optimization and in vitro characterization. Nanomaterials (Basel). 2016;6(6):116. doi: 10.3390/nano6060116.
39. Desai NP, Tao C, Yang A, Louie L, Zheng T, Yao Z, et al. Protein Stabilized Pharmacologically Active Agents, Methods

for the Preparation Thereof and Methods for the Use Thereof. Google Patents; 2004.
40. Hobbs SK, Monsky WL, Yuan F, Roberts WG, Griffith L, Torchilin VP, et al. Regulation of transport pathways in tumor vessels: role of tumor type and microenvironment. Proc Natl Acad Sci U S A. 1998;95(8):4607-12. doi: 10.1073/pnas.95.8.4607.
41. Yuan F, Dellian M, Fukumura D, Leunig M, Berk DA, Torchilin VP, et al. Vascular permeability in a human tumor xenograft: molecular size dependence and cutoff size. Cancer Res. 1995;55(17):3752-6.
42. Zhao X, Liu R, Chi Z, Teng Y, Qin P. New insights into the behavior of bovine serum albumin adsorbed onto carbon nanotubes: comprehensive spectroscopic studies. J Phys Chem B. 2010;114(16):5625-31. doi: 10.1021/jp100903x.
43. Hospes M, Hendriks J, Hellingwerf KJ. Tryptophan fluorescence as a reporter for structural changes in photoactive yellow protein elicited by photo-activation. Photochem Photobiol Sci. 2013;12(3):479-88. doi: 10.1039/c2pp25222h.
44. Kratz F. Albumin as a drug carrier: design of prodrugs, drug conjugates and nanoparticles. J Control Release. 2008;132(3):171-83. doi: 10.1016/j.jconrel.2008.05.010.
45. Luo J, Xiao K, Li Y, Lee JS, Shi L, Tan YH, et al. Well-defined, size-tunable, multifunctional micelles for efficient paclitaxel delivery for cancer treatment. Bioconjug Chem. 2010;21(7):1216-24. doi: 10.1021/bc1000033.
46. Tiruppathi C, Song W, Bergenfeldt M, Sass P, Malik AB. Gp60 activation mediates albumin transcytosis in endothelial cells by tyrosine kinase-dependent pathway. J Biol Chem. 1997;272(41):25968-75. doi: 10.1074/jbc.272.41.25968.
47. Vigneshwaran N, Kathe AA, Varadarajan PV, Nachane RP, Balasubramanya RH. Silver-protein (core-shell) nanoparticle production using spent mushroom substrate. Langmuir. 2007;23(13):7113-7. doi: 10.1021/la063627p.
48. Takabatake D, Fujita T, Shien T, Kawasaki K, Taira N, Yoshitomi S, et al. Tumor inhibitory effect of gefitinib (ZD1839, Iressa) and taxane combination therapy in EGFR-overexpressing breast cancer cell lines (MCF7/ADR, MDA-MB-231). Int J Cancer. 2007;120(1):181-8. doi: 10.1002/ijc.22187.
49. Piao MJ, Kang KA, Lee IK, Kim HS, Kim S, Choi JY, et al. Silver nanoparticles induce oxidative cell damage in human liver cells through inhibition of reduced glutathione and induction of mitochondria-involved apoptosis. Toxicol Lett. 2011;201(1):92-100. doi: 10.1016/j.toxlet.2010.12.010.
50. Park MV, Neigh AM, Vermeulen JP, de la Fonteyne LJ, Verharen HW, Briedé JJ, et al. The effect of particle size on the cytotoxicity, inflammation, developmental toxicity and genotoxicity of silver nanoparticles. Biomaterials. 2011;32(36):9810-7. doi: 10.1016/j.biomaterials.2011.08.085.
51. Gurunathan S, Han JW, Dayem AA, Eppakayala V, Park JH, Cho SG, et al. Green synthesis of anisotropic silver nanoparticles and its potential cytotoxicity in human breast cancer cells (MCF-7). J Ind Eng Chem. 2013;19(5):1600-5. doi: 10.1016/j.jiec.2013.01.029.
52. Mirtsching B, Cosgriff T, Harker G, Keaton M, Chidiac T, Min M. A phase II study of weekly nanoparticle albumin-bound paclitaxel with or without trastuzumab in metastatic breast cancer. Clin Breast Cancer. 2011;11(2):121-8. doi: 10.1016/j.clbc.2011.03.007.
53. Zenoni M, Maschio S. Process for Producing Nanoparticles of Paclitaxel and Albumin. Google Patents; 2003.
54. Desai N. Challenges in development of nanoparticle-based therapeutics. AAPS J. 2012;14(2):282-95. doi: 10.1208/s12248-012-9339-4.
55. Sjöström B, Bergenståhl B, Lindberg M, Rasmuson ÅC. The formation of submicron organic particles by precipitation in an emulsion. J Dispers Sci Technol. 1994;15(1):89-117. doi: 10.1080/01932699408943545.
56. Rahman MA, Hussain A. Anti-cancer activity and apoptosis inducing effect of methanolic extract of *Cordia dichotoma* against human cancer cell line. Bangladesh J Pharmacol. 2015;10(1):27-34. doi: 10.3329/bjp.v10i1.20883.
57. Wyllie AH. Glucocorticoid-induced thymocyte apoptosis is associated with endogenous endonuclease activation. Nature. 1980;284(5756):555-6. doi: 10.1038/284555a0.
58. Asharani P, Sethu S, Lim HK, Balaji G, Valiyaveettil S, Hande MP. Differential regulation of intracellular factors mediating cell cycle, DNA repair and inflammation following exposure to silver nanoparticles in human cells. Genome Integr. 2012;3(1):2. doi: 10.1186/2041-9414-3-2.
59. Demidenko ZN, Kalurupalle S, Hanko C, Lim CU, Broude E, Blagosklonny MV. Mechanism of G1-like arrest by low concentrations of paclitaxel: next cell cycle p53-dependent arrest with sub G1 DNA content mediated by prolonged mitosis. Oncogene. 2008;27(32):4402-10. doi: 10.1038/onc.2008.82.
60. Shu CH, Yang WK, Shih YL, Kuo ML, Huang TS. Cell cycle G2/M arrest and activation of cyclin-dependent kinases associated with low-dose paclitaxel-induced sub-G1 apoptosis. Apoptosis. 1997;2(5):463-70. doi: 10.1023/a:1026422111457.
61. Das A, Banik NL, Ray SK. Retinoids induced astrocytic differentiation with down regulation of telomerase activity and enhanced sensitivity to Taxol for apoptosis in human glioblastoma T98G and U87MG cells. J Neurooncol. 2008;87(1):9-22. doi: 10.1007/s11060-007-9485-1.
62. Hong GY, Jeong YI, Lee SJ, Lee E, Oh JS, Lee HC. Combination of paclitaxel- and retinoic acid-incorporated nanoparticles for the treatment of CT-26 colon carcinoma. Arch Pharm Res. 2011;34(3):407-17. doi: 10.1007/s12272-011-0308-8.
63. Ridwelski K, Gebauer T, Fahlke J, Kröning H, Kettner E, Meyer F, et al. Combination chemotherapy with docetaxel and cisplatin for locally advanced and metastatic gastric cancer. Ann Oncol. 2001;12(1):47-51. doi: 10.1023/a:1008328501128.
64. Sarkar K, Yang H. Encapsulation and extended release of anti-cancer anastrozole by stealth nanoparticles. Drug Deliv. 2008;15(5):343-6. doi: 10.1080/10717540802035343.
65. Sofou S. Radionuclide carriers for targeting of cancer. Int J Nanomedicine. 2008;3(2):181-99. doi: 10.2147/ijn.s2736.
66. Torchilin V. Antibody-modified liposomes for cancer chemotherapy. Expert Opin Drug Deliv. 2008;5(9):1003-25. doi: 10.1517/17425247.5.9.1003.
67. Park HJ, Kim JY, Kim J, Lee JH, Hahn JS, Gu MB, et al. Silver-ion-mediated reactive oxygen species generation affecting bactericidal activity. Water Res. 2009;43(4):1027-32. doi: 10.1016/j.watres.2008.12.002.
68. Carlson C, Hussain SM, Schrand AM, Braydich-Stolle LK, Hess KL, Jones RL, et al. Unique cellular interaction of silver nanoparticles: size-dependent generation of reactive oxygen species. J Phys Chem B. 2008;112(43):13608-19. doi: 10.1021/jp712087m.
69. Sriram N, Kalayarasan S, Sudhandiran G. Enhancement of antioxidant defense system by epigallocatechin-3-gallate during bleomycin induced experimental pulmonary fibrosis. Biol Pharm Bull. 2008;31(7):1306-11. doi: 10.1248/bpb.31.1306.
70. Azizi M, Ghourchian H, Yazdian F, Dashtestani F, Alizadeh Zeinabad H. Cytotoxic effect of albumin coated copper nanoparticle on human breast cancer cells of MDA-MB 231. PLoS One. 2017;12(11):e0188639. doi: 10.1371/journal.

pone.0188639.
71. Ding X, Hua Y, Chen Y, Zhang C, Kong X. Heavy metal complexation of thiol-containing peptides from soy glycinin hydrolysates. Int J Mol Sci. 2015;16(4):8040-58. doi: 10.3390/ijms16048040.
72. Kratz F, Senter P, Steinhagen H. Drug Delivery in Oncology: From Basic Research to Cancer Therapy. John Wiley & Sons; 2013.
73. Otagiri M, Chuang VT. Albumin in Medicine. Springer; 2016.
74. Frei E. Albumin binding ligands and albumin conjugate uptake by cancer cells. Diabetol Metab Syndr. 2011;3(1):11. doi: 10.1186/1758-5996-3-11.
75. Shakibaei M, John T, Schulze-Tanzil G, Lehmann I, Mobasheri A. Suppression of NF-κB activation by curcumin leads to inhibition of expression of cyclo-oxygenase-2 and matrix metalloproteinase-9 in human articular chondrocytes: implications for the treatment of osteoarthritis. Biochem Pharmacol. 2007;73(9):1434-45. doi: 10.1016/j.bcp.2007.01.005.